Journal of Zhejiang University-SCIENCE A 2026 27(1):76-86
www.jzus.zju.edu.cn; www.springer.com/journal/11582
E-mail: jzus_a@zju.edu.cn

Research Article
https://doi.org/10.1631/jzus.A2500400

Design and energy function determination of a memristor-coupled circuit representing a two-dimensional chaotic map

Feifei YANG[1], Xinlin SONG[2]✉, Jia HE[1], Huiping YIN[1]

[1]*College of Artificial Intelligence and Computer Science, Xi'an University of Science and Technology, Xi'an 710054, China*
[2]*College of Science, Xi'an University of Science and Technology, Xi'an 710054, China*

Abstract: The modeling and dynamical analysis of discrete chaotic systems is a vital research field, and various chaotic maps have been developed using mathematical and control-theoretic approaches. However, physical circuit design of mathematically defined discrete chaotic systems and the computation of their energy functions remain challenging and open problems. In this study, a two-dimensional (2D) chaotic map is constructed using an open-loop modulation coupling method, and its dynamical characteristics are analyzed using bifurcation diagrams. Lyapunov exponents (LEs) and spectral entropy (SE) complexity are also inspected under different parameter configurations. Furthermore, the proposed chaotic map is expressed using two distinct physical memristive circuits: one is composed of a magnetic flux-controlled memristor, a nonlinear resistor, and a capacitor; the other utilizes a charge-controlled memristor, a nonlinear resistor, and an inductor. Moreover, two energy functions are derived from the two memristor-coupled circuits for the proposed chaotic map. The results demonstrate that the mathematical model of the discrete chaotic system can be effectively expressed through these two nonlinear circuits. Our study offers a theoretical foundation and viable methodology for the physical circuit representation of discrete chaotic systems and determination of their energy functions.

Key words: Modulation coupling; Chaotic map; Dynamics analysis; Energy function; Memristor circuit

1 Introduction

Discrete chaotic systems are typically represented by mathematical models that capture chaotic behaviors in discrete-time frameworks. These discrete chaotic systems exhibit strong nonlinearity and can produce complex dynamical behavior and high levels of randomness. Such features make them widely applicable in areas such as random number generation (Tutueva et al., 2020; Umar et al., 2024; Wu and Zhou, 2024) and image encryption (Sameh et al., 2024; Jackson and Perumal, 2025; Verma and Kumar, 2025). As a result, the design and application of discrete chaotic systems continue to attract significant research interest.

✉ Xinlin SONG, xinlinsong@xust.edu.cn
Feifei YANG, https://orcid.org/0000-0002-1649-1225
Xinlin SONG, https://orcid.org/0000-0001-5467-544X
Huiping YIN, https://orcid.org/0000-0001-8236-0621

Received Aug. 27, 2025; Revision accepted Oct. 21, 2025;
Crosschecked Dec. 4, 2025; Online first Dec. 19, 2025

In recent years, diverse chaotic maps and neuron maps have been developed and their dynamical behaviors have been systematically studied. Notable examples include two-dimensional (2D) chaotic maps (Peng et al., 2020), 2D hyperchaotic maps (Ma et al., 2024), three-dimensional (3D) chaotic maps (Wang et al., 2025), memristive chaotic maps (Peng et al., 2021; Li KS et al., 2024; Xiang et al., 2024), memristive hyperchaotic maps (Bao et al., 2021; Ma et al., 2022; Zhang et al., 2023), neuron maps (Luo and Flanagan, 2007; Ibarz et al., 2011; Narayanan and Johnston, 2012), and memristive neuron maps (Muni et al., 2022; Ramakrishnan et al., 2022; Wang Z et al., 2024). Furthermore, chaotic maps have been widely applied in the design of image encryption algorithms–specific work includes chaotic map-based image encryption algorithms (Akraam et al., 2023; Li, 2024; Jackson and Perumal, 2025), image encryption schemes employing hyperchaotic maps (Alexan et al., 2023a, 2023b; Lai and Liu, 2023), image encryption algorithms using memristive chaotic maps (Peng et al., 2023; Liu et al., 2024; Wang C et al., 2024), image encryption approaches

grounded in neuron maps (Alexan et al., 2023a; Gao et al., 2025), and image encryption methods incorporating memristive neuron maps (Xu et al., 2023).

These chaotic maps and neuron maps are derived from improvements to existing discrete systems through mathematical methods. Some chaotic maps and neuron maps have also been established from a physical perspective. For example, Yang et al. (2024a, 2024c) proposed two 2D memristive chaotic maps and a 3D memristive chaotic map by using two simple memristor-coupled circuits and a dual memristor-coupled circuit. Similarly, two memristive map neuron models were constructed using memristive neuron circuits (Yang et al., 2024b; Chen et al., 2025). Jia et al. (2024) proposed a memristive neuron map via a memristor-coupled circuit and studied its energy properties and adaptive behavior. Moreover, Li YN et al. (2024) designed a memristive map neuron from a memristor-coupled circuit and investigated its adaptive dynamics. In (Wang BC et al., 2024; Lei and Ma, 2025), memristive neuron maps were implemented using memristor-coupled circuits, with a focus on coherent resonance phenomena. Detailed methodologies for energy computation in memristive maps can be found in references (Guo et al., 2023, 2024). In fact, some hyperchaotic maps with neural models have been applied in data security (Gabr et al., 2024) and image encryption algorithms (Alexan et al., 2023a; Gabr et al., 2023).

Research on these aforementioned map systems demonstrates that map models can be successfully established through both mathematical and physical methods. However, analog circuit design of map systems and the computation of their energy functions remain unresolved challenges. In this paper, we introduce the physical circuit representation and energy calculation methods for general discrete systems. This study contributes to analog circuit design of chaotic map models and associated energy calculations, offering an effective approach for validating the physical reliability of mathematically defined map systems. The main highlights of this work are:

(1) A 2D model of a chaotic map is built using an open-loop modulation coupling method.

(2) The proposed chaotic map is expressed by applying two different memristor-coupled circuits.

(3) Two energy functions for the proposed chaotic map are derived from the two different memristor-coupled circuits.

2 Model of a chaotic map and its dynamics

As is well known, even the simplest nonlinear oscillatory circuit can be described by a system of two nonlinear differential equations. Therefore, for a discrete system to be physically realizable via analog circuits, it must be at least 2D. For simplicity, in this study, we specifically focus on the circuit design of a 2D chaotic map and its energy function. A 2D chaotic map is generated by applying an open-loop modulation coupling method, and its structural diagram is shown in Fig. 1.

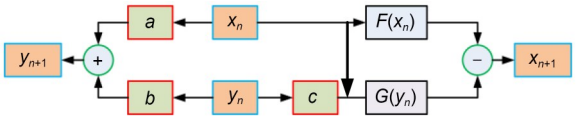

Fig. 1 Structural diagram of an open-loop modulation coupling method. Variables will be given in the maintext

The structural diagram of an open-loop modulation coupling system in Fig. 1 can be expressed as follows:

$$\begin{cases} x_{n+1}=F(x_n)-cx_nG(y_n), \\ y_{n+1}=by_n+ax_n, \end{cases} \tag{1}$$

where a, b, and c represent the coefficients. (x_n, y_n) denotes the iterative variable. $F(x_n)$ and $G(y_n)$ can be selected as a one-dimensional chaotic map, a linear function, or a nonlinear function. In this study, $F(x_n)$ is defined as a nonlinear function, and $G(y_n)$ is chosen as a linear function. Thus, the 2D map system can be described by

$$\begin{cases} x_{n+1}=\mu_1 x_n-\mu_2 x_n^2-cx_ny_n, \\ y_{n+1}=by_n+ax_n, \end{cases} \tag{2}$$

where μ_1 and μ_2 are the parameters of the nonlinear function $F(x_n)$.

To further investigate the dynamical behaviors of the map given in Eq. (2), based on parameters and initial value of the logistic map, the parameters are fixed at μ_1=μ_2=3.9 and c=0.12, with the initial value set to (0.1, 0.2). The bifurcation diagrams and Lyapunov exponents (LEs) are computed for different values of the parameters (a, b), and the results are shown in Fig. 2.

The results demonstrate that the dynamical behaviors of the map given in Eq. (2) can be modulated

by varying the parameters. For instance, chaotic attractors and various types of periodic patterns emerge under different parameter values. Furthermore, phase trajectories corresponding to different values of the parameter b are illustrated in Fig. 3.

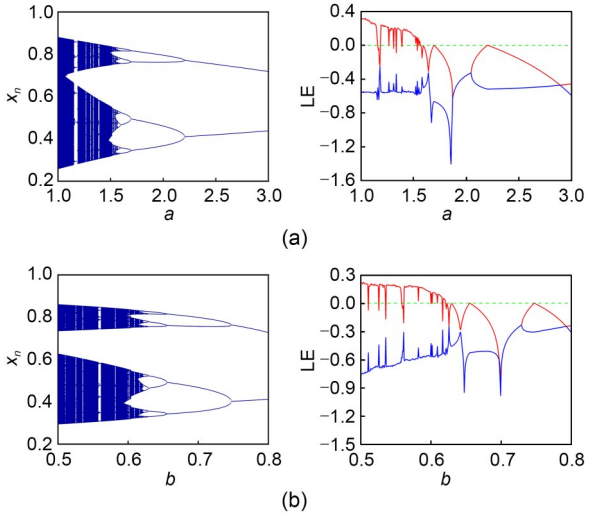

Fig. 2 Bifurcation diagrams of variable x_n and LEs by adjusting the values of parameters (a, b): (a) a∈[1, 3], b=0.6; (b) b∈[0.5, 0.8], a=1.5

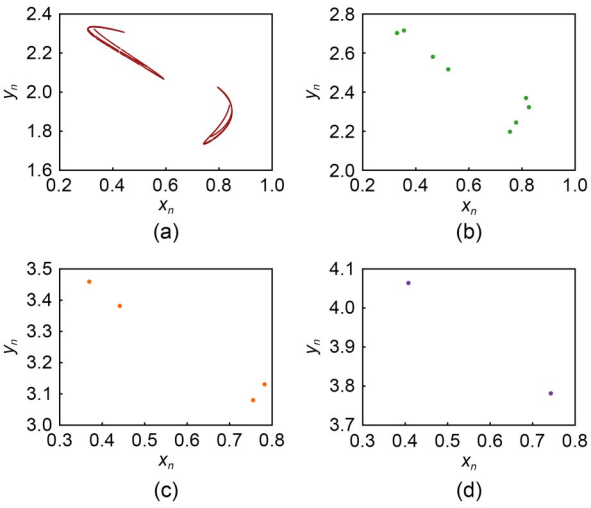

Fig. 3 Phase trajectories under different values of parameter b: (a) b=0.55, a=1.5; (b) b=0.63, a=1.5; (c) b=0.73, a=1.5; (d) b=0.78, a=1.5

As shown in Fig. 3, chaotic attractors and various types of periodic attractors are obtained by adjusting the parameter b. These results confirm that the map defined by Eq. (2) exhibits chaotic behavior and possesses rich nonlinear dynamical features, including period-2, period-4, and period-8 orbits. The influence of other parameters on the system dynamics is further apparent following validation with a two-parameter bifurcation. Under the same initial values as specified above, the corresponding bifurcation diagrams are presented in Fig. 4.

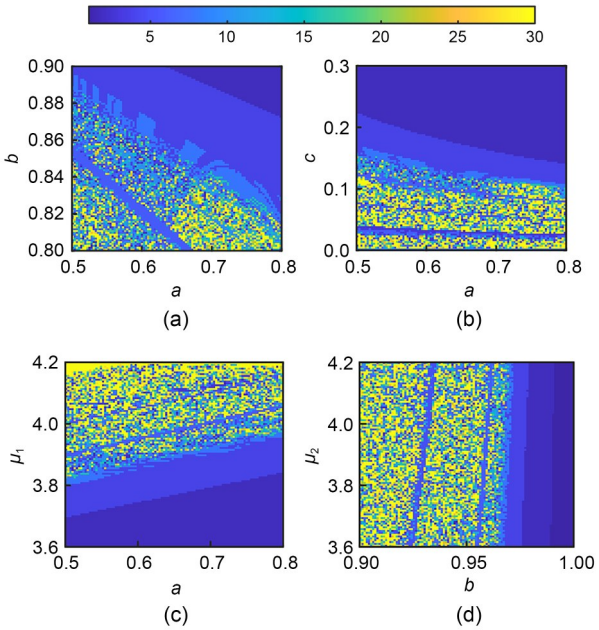

Fig. 4 Bifurcation diagrams of variable x_n from adjustment of the parameters: (a) μ_1=μ_2=3.9, c=0.12; (b) μ_1=μ_2=3.9, b=1.5; (c) b=0.85, c=0.12, μ_2=3.9; (d) a=0.15, c=0.12, μ_1=3.9. References to color refer to the online version of this figure

In Fig. 4, the yellow regions correspond to chaotic states, while other colors represent distinct periodic states. Different parameter combinations can induce either periodic or chaotic dynamics. Complexity measures such as spectral entropy (SE) can also be used to distinguish between chaotic and periodic behaviors in nonlinear systems, as chaotic modes generally exhibit higher complexity values, whereas periodic modes yield lower ones. To further analyze the dynamics of the chaotic map given in Eq. (2), the SE complexity is computed under fixed parameter conditions and an initial value of (0.1, 0.2). The resulting two-parameter SE complexity diagram is presented in Fig. 5.

In Fig. 5, chaotic patterns exhibit higher SE complexity values (indicated in red), whereas periodic modes correspond to lower values. These results demonstrate that the nonlinear dynamics of the chaotic map given in Eq. (2) can be effectively regulated through two-parameter variation, with chaotic behavior occurring across a broad range of parameter values.

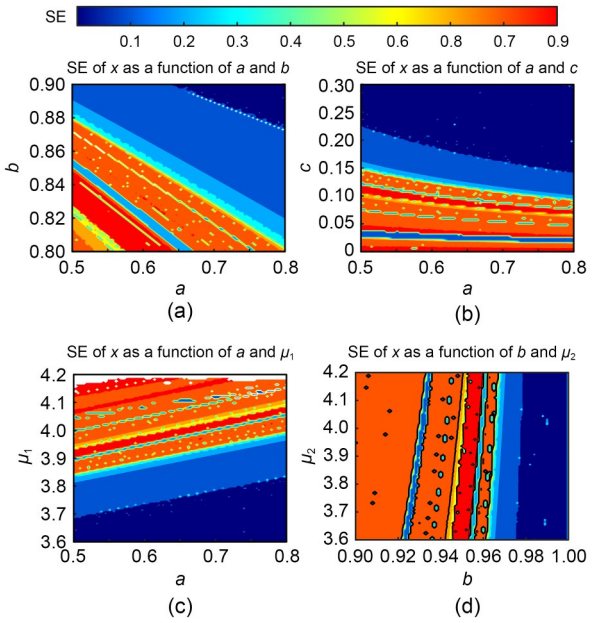

Fig. 5 SE complexity of variable x_n by adjusting parameter values: (a) μ_1=μ_2=3.9, c=0.12; (b) μ_1=μ_2=3.9, b=1.5; (c) b=0.85, c=0.12, μ_2=3.9; (d) a=0.15, c=0.12, μ_1=3.9. References to color refer to the online version of this figure

To more deeply explore the new discrete chaotic map sequences, which display greater randomness, we set three different initial state values and calculate the resulting SE complexity values, repeating this process three times and taking the average SE value. For the chaotic maps, which include examples such as 2D sine logistic modulation map (2D-SLMM) from other references (Hua et al., 2015), the SE complexity comparison results are shown in Table 1. It is clear that the proposed discrete chaotic map has a higher SE complexity value, and therefore exhibits greater randomness.

In chaotic systems, even the slightest differences (whether it be minor variations in the system's own parameters or in the initial state) will be exponentially magnified as the system evolves, leading to the final outcome being substantially different from the original situation, and completely unpredictable. To investigate the sensitivity of the chaotic map given in Eq. (2) to its parameters and initial values, the parameters are fixed at b=1.5, c=0.12, μ_1=μ_2=3.9, and the initial value is set to y_0=0.2, then the variable x is calculated for different a parameter values and initial variable x_0 values; the results are shown in Fig. 6.

The results in Fig. 6 indicate that two nearly identical parameters and initial states, after evolving for a sufficient period, will have completely different trajectories and show no similarities. Therefore, the chaotic map system in Eq. (2) exhibits sensitivity to changes in parameters and initial values.

3 Circuit expression of a chaotic map

Initially, the map equations given in Eq. (2) can be linearly transformed into an equivalent form of differential equations. The variables in Eq. (2) are defined as follows:

$$w_n=\frac{1+\Delta\tau}{\Delta\tau}x_n,\ u_n=\frac{1+\Delta\tau}{\Delta\tau}y_n. \tag{3}$$

As a result, Eq. (2) is updated by

$$\begin{cases} w_{n+1}\dfrac{\Delta\tau}{1+\Delta\tau}=\mu\left(w_n\dfrac{\Delta\tau}{1+\Delta\tau}-\left(w_n\dfrac{\Delta\tau}{1+\Delta\tau}\right)^2\right)-\\ \qquad cw_n\dfrac{\Delta\tau}{1+\Delta\tau}u_n\dfrac{\Delta\tau}{1+\Delta\tau},\\ u_{n+1}\dfrac{\Delta\tau}{1+\Delta\tau}=bu_n\dfrac{\Delta\tau}{1+\Delta\tau}+aw_n\dfrac{\Delta\tau}{1+\Delta\tau}. \end{cases} \tag{4}$$

Eq. (4) can then be rewritten as follows:

$$\begin{cases} w_{n+1}\dfrac{\Delta\tau}{1+\Delta\tau}-w_n\dfrac{\Delta\tau}{1+\Delta\tau}=\\ \qquad \mu\left(w_n\dfrac{\Delta\tau}{1+\Delta\tau}-\left(w_n\dfrac{\Delta\tau}{1+\Delta\tau}\right)^2\right)-\\ \qquad cw_n\dfrac{\Delta\tau}{1+\Delta\tau}u_n\dfrac{\Delta\tau}{1+\Delta\tau}-w_n\dfrac{\Delta\tau}{1+\Delta\tau},\\ u_{n+1}\dfrac{\Delta\tau}{1+\Delta\tau}-u_n\dfrac{\Delta\tau}{1+\Delta\tau}=\\ \qquad bu_n\dfrac{\Delta\tau}{1+\Delta\tau}+aw_n\dfrac{\Delta\tau}{1+\Delta\tau}-u_n\dfrac{\Delta\tau}{1+\Delta\tau}. \end{cases} \tag{5}$$

Table 1 SE complexity value comparison results

Map model	Parameter value	SE1	SE2	SE3	Average SE	Ranking
This paper	a=0.15, c=0.12, μ_1=μ_2=3.9, b=0.91	0.888	0.887	0.889	0.888	1
Sine (Hua et al., 2015)	a_0=1, ω=π	0.868	0.871	0.859	0.866	2
2D-SLMM (Hua et al., 2015)	a=1	0.812	0.819	0.705	0.779	3
2D-SLMM (Hua et al., 2015)	μ=1	0.363	0.363	0.375	0.367	4

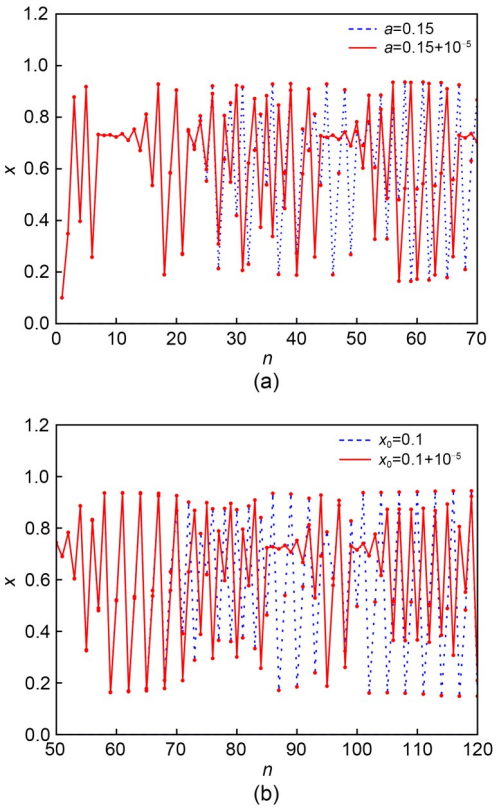

Fig. 6 Evolution of variable x under different a parameter values and initial values: (a) parameter a is changed by 10^{-5}; (b) initial value of x_0 is changed by 10^{-5}

Using $\mathrm{d}x/\mathrm{d}\tau=(x_{n+1}-x_n)/\Delta\tau$, Eq. (5) is updated as follows:

$$\begin{cases}\dfrac{\mathrm{d}w}{\mathrm{d}\tau}=\dfrac{1}{\Delta\tau}\left(\left(\mu_1 w-\mu_2 w^2\dfrac{\Delta\tau}{1+\Delta\tau}\right)-cwu\dfrac{\Delta\tau}{1+\Delta\tau}-w\right),\\ \dfrac{\mathrm{d}u}{\mathrm{d}\tau}=\dfrac{1}{\Delta\tau}(bu+aw-u).\end{cases}\tag{6}$$

Then, Eq. (6) can be simplified to:

$$\begin{cases}\dfrac{\mathrm{d}w}{\mathrm{d}\tau}=\mu_1' w-\mu_2' w^2-c'wu,\\ \dfrac{\mathrm{d}u}{\mathrm{d}\tau}=b'u+a'w,\end{cases}\tag{7}$$

where

$$\mu_1'=\frac{\mu_1-1}{\Delta\tau},\ \mu_2'=\frac{\mu_2}{1+\Delta\tau},\ c'=\frac{c}{1+\Delta\tau},\ b'=\frac{b-1}{\Delta\tau},\ a'=\frac{a}{\Delta\tau}.\tag{8}$$

Next, the physical dimensions of the variables in Eq. (7) are defined as follows:

$$w=\frac{v}{v_0},\ u=\frac{\varphi}{\rho C v_0},\ \tau=\frac{t}{\rho C},\tag{9}$$

where v_0 is the reference voltage, C is the capacitance of a capacitor, and ρ is the resistance of a resistor. Then, Eq. (7) can be updated by

$$\begin{cases}C\dfrac{\mathrm{d}v}{\mathrm{d}t}=\dfrac{1}{\rho}\left(\mu_1' v-\mu_2'\dfrac{v^2}{v_0}\right)-\dfrac{c'}{C\rho^2 v_0}v\varphi,\\ \dfrac{\mathrm{d}\varphi}{\mathrm{d}t}=\dfrac{b'}{C\rho v_0^2}\varphi+\dfrac{a'}{v_0^2}v.\end{cases}\tag{10}$$

Subsequently, Eq. (10) can simplified as follows:

$$\begin{cases}C\dfrac{\mathrm{d}v}{\mathrm{d}t}=\dfrac{1}{\rho}\left(\mu_1' v-\mu_2'\dfrac{v^2}{v_0}\right)-\alpha v\varphi,\\ \dfrac{\mathrm{d}\varphi}{\mathrm{d}t}=\beta\varphi+\gamma v,\end{cases}\tag{11}$$

where

$$\alpha=\frac{c'}{C\rho^2 v_0},\ \beta=\frac{b'}{C\rho v_0^2},\ \gamma=\frac{a'}{v_0^2}.\tag{12}$$

In fact, the higher-order terms in Eq. (11) can be defined as a nonlinear resistor (NR), and the current across the nonlinear resistor i_{NR} is described as:

$$i_{\mathrm{NR}}=-\frac{1}{\rho}\left(\mu_1' v-\mu_2'\frac{v^2}{v_0}\right),\tag{13}$$

where ρ is the resistance of a nonlinear resistor, (μ_1', μ_2') denotes the dimensionless parameters of a nonlinear resistor, v_0 is the cut-off voltage, and v is the voltage across the nonlinear resistor. The cross term and second equation in Eq. (11) can be defined as a magnetic flux-controlled memristor, of which the current i_{M} is expressed by

$$\begin{cases}i_{\mathrm{M}}=\alpha v\varphi,\\ \dfrac{\mathrm{d}\varphi}{\mathrm{d}t}=\beta\varphi+\gamma v,\end{cases}\tag{14}$$

where φ is the magnetic flux, v is the voltage across the memristor, and (α, β, γ) denotes the parameters related to the memristor material. Based on Eq. (11)

and Kirchhoff's law, the current relationship between electronic components in a circuit is described by

$$i_{\mathrm{M}}=-i_{\mathrm{NR}}-i_{\mathrm{C}}, \tag{15}$$

where i_{C} is the current of the capacitor.

Incorporating all of this, the magnetic flux-controlled memristor-coupled circuit corresponding to the discrete system presented in Eq. (2) is designed, with a diagram shown in Fig. 7.

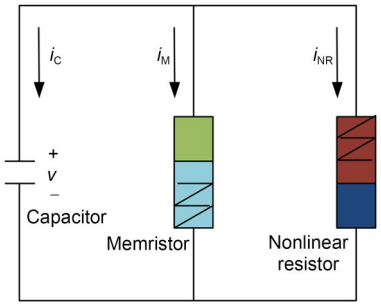

Fig. 7 Magnetic flux-controlled memristor-coupled circuit without an inductor

The map system defined from the mathematical model is thus expressed using a circuit constructed from physical electronic components, including a nonlinear resistor, a magnetic flux-controlled memristor, and capacitors. Furthermore, the physical dimensions of the variables in Eq. (7) can be defined by

$$w=\frac{\rho i_{\mathrm{L}}}{v_0},\ u=\frac{q\rho^2}{Lv_0},\ \tau=\frac{\rho t}{L}, \tag{16}$$

where q is the charge, i_{L} is the current across the nonlinear resistor, v_0 is the reference voltage, L is the inductance of the induction coil, and ρ denotes the resistance of the resistor. Then Eq. (7) can be updated by

$$\begin{cases} L\dfrac{\mathrm{d}i_{\mathrm{L}}}{\mathrm{d}t}=\dfrac{\mu_1'}{v_0^2}\rho i_{\mathrm{L}}-\dfrac{\mu_2'}{v_0^2}\dfrac{\rho^2 i_{\mathrm{L}}^2}{v_0}-\dfrac{\rho^3 c'}{Lv_0^3}qi_{\mathrm{L}}, \\ \dfrac{\mathrm{d}q}{\mathrm{d}t}=\dfrac{b'\rho}{L}q+a'i_{\mathrm{L}}. \end{cases} \tag{17}$$

Furthermore, Eq. (17) can be simplified as follows:

$$\begin{cases} L\dfrac{\mathrm{d}i_{\mathrm{L}}}{\mathrm{d}t}=\eta\rho i_{\mathrm{L}}-\varsigma\dfrac{\rho^2 i_{\mathrm{L}}^2}{v_0}-\kappa qi_{\mathrm{L}}, \\ \dfrac{\mathrm{d}q}{\mathrm{d}t}=\delta q+\lambda i_{\mathrm{L}}, \end{cases} \tag{18}$$

where

$$\eta=\frac{\mu_1'}{v_0^2},\ \varsigma=\frac{\mu_2'}{v_0^2},\ \kappa=\frac{\rho^3 c'}{Lv_0^3},\ \delta=\frac{b'\rho}{L},\ \lambda=a'. \tag{19}$$

The higher-order terms in Eq. (18) are considered as a nonlinear resistor, and its voltage across is defined as:

$$v_{\mathrm{NR}}=\eta\rho i_{\mathrm{L}}-\varsigma\frac{\rho^2 i_{\mathrm{L}}^2}{v_0}, \tag{20}$$

where (η, ς) denotes the dimensionless parameters of the nonlinear resistor, and v_0 denotes the cut-off voltage. That is, a high-order nonlinear term can be realized using a nonlinear resistor and two closed loops (three branch circuits) in a neural circuit to perform signal processing and functional regulation.

Indeed, functional regulation from the nonlinear term can be incorporated into a charge-controlled memristor (CCM) when the nonlinear resistor is broken or unavailable. In this way, a simpler neural circuit in one closed loop is proposed in Fig. 8, and the CCM activates the regulation of the energy flow in a nonlinear manner. The cross term and second equation in Eq. (18) make up a charge-controlled memristor, of which the voltage v_{M} is defined as follows:

$$\begin{cases} v_{\mathrm{M}}=\kappa qi_{\mathrm{L}}, \\ \dfrac{\mathrm{d}q}{\mathrm{d}t}=\delta q+\lambda i_{\mathrm{L}}, \end{cases} \tag{21}$$

where $(\kappa, \delta, \lambda)$ denotes the parameters related to the memristor material. Based on Eq. (18) and Kirchhoff's law, the voltage relationship between the electronic components in the circuit is:

$$v_{\mathrm{L}}=v_{\mathrm{NR}}-v_{\mathrm{M}}. \tag{22}$$

Therefore, the charge-controlled memristor-coupled circuit corresponding to the discrete system given by Eq. (2) is designed as shown in Fig. 8.

Therefore, the map system defined from the mathematical model can be expressed using a circuit implemented with physical electronic components, including a nonlinear resistor, a charge-controlled memristor, and an induction coil.

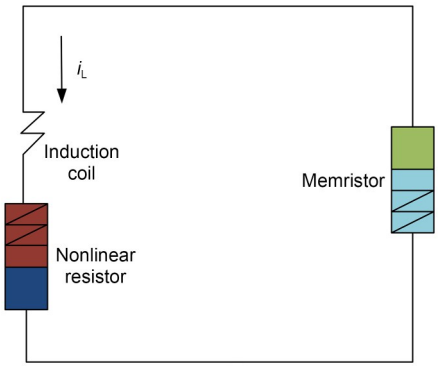

Fig. 8 Charge-controlled memristor-coupled circuit without a capacitor

4 Energy function of the map system

In classical physics, energy is conserved, but the vast majority of chaotic systems are dissipative (meaning energy decreases or diverges over time), and energy is not conserved in the traditional sense. The energy referred to here is a broad, mathematical analogue or pseudo-energy function. It is not a physical Joule but a measure of the activity level, excitation level, or nonlinearity intensity of a system's state. This provides a novel and abstract energy perspective for understanding chaos. By using mathematical methods (such as embedding methods), it can be proved that a dissipative chaotic system can be represented as a projection or subsystem of a higher-dimensional, energy-conserving system. This reveals the deeper regularity that might be hidden behind chaos. That is, randomness, dissipation, and unpredictability may stem from a higher-dimensional, regular, and conservational dynamic process. This has greatly deepened the understanding of the essence of chaos.

The constructed energy function evolves over time, and its statistical properties (such as the variance of energy, volatility, and entropy value) can serve as new and more robust features to effectively distinguish between periodic, chaotic, and random movements; they can even be used to quantify the intensity of chaos. Chaotic states typically correspond to intense and irregular fluctuations in energy, while periodic states correspond to stable and periodic changes in energy.

Chaos control: If an energy function is available, the control problem can be transformed into a more intuitive energy control problem. By applying a small perturbation, the "energy" of the system can be stabilized at a desired low value (corresponding to a periodic orbit). This provides a clear objective function for controller design.

Synchronization of chaos: The goal is to make the trajectories of two or more chaotic systems consistent. By reducing the energy difference between the systems to zero, synchronization can be achieved. This task has applied value in fields such as secure communication and neural network synchronization.

Therefore, studying the energy of discrete chaotic systems and the construction of energy functions is a promising research direction that applies classical physical concepts to modern nonlinear science. It is not only an important theoretical idea, but also a practical tool. In this work, the energy function of the chaotic map given in Eq. (2) is defined through the memristor-coupled circuits shown in Figs. 6 and 7.

As seen in Fig. 7, the energy storage component consists of a magnetic flux-controlled memristor and a capacitor. Therefore, the physical field energy of this component can be calculated as follows:

$$W=\frac{1}{2}Cv^2+\frac{1}{2}\varphi i_{\mathrm{M}}, \tag{23}$$

where v is the voltage of the capacitor.

According to Eq. (14) and Fig. 7, Eq. (23) can be updated by:

$$W=\frac{1}{2}Cv^2+\frac{1}{2}\alpha\varphi^2 v. \tag{24}$$

Furthermore, based on Eqs. (8), (9), and (12), the dimensionless energy function corresponding to the physical field energy in Eq. (24) is described as follows:

$$H=\frac{W}{Cv_0^2}=\frac{1}{2}w^2+\frac{1}{2}c'u^2w. \tag{25}$$

Therefore, the energy function of the chaotic map given in Eq. (2) can be expressed by:

$$H_{n+1}=\frac{1}{2}x_n^2+\frac{1}{2}cy_n^2x_n. \tag{26}$$

In Fig. 8, the energy storage component consists of a charge-controlled memristor and an inductor. Therefore, the physical field energy of this component can be determined as:

$$W=\frac{1}{2}Li_{\mathrm{L}}^2+\frac{1}{2}qv_{\mathrm{M}}. \tag{27}$$

According to Eq. (21), Eq. (27) can be updated by:

$$W=\frac{1}{2}Li_{\mathrm{L}}^2+\frac{1}{2}\kappa qi_{\mathrm{L}}^2. \tag{28}$$

Moreover, based on Eqs. (16) and (19), the dimensionless energy function corresponding to the physical field energy in Eq. (27) is described as follows:

$$H=\frac{W}{\frac{v_0^2L}{\rho^2}}=\frac{1}{2}w^2+\frac{1}{2}c'u^2w. \tag{29}$$

Consequently, the energy function of the chaotic map given in Eq. (2) can be expressed by:

$$H_{n+1}=\frac{1}{2}x_n^2+\frac{1}{2}cy_n^2x_n. \tag{30}$$

In order to further investigate the energy distribution of the mapping dynamics, sequence evolution diagrams corresponding to different dynamic behaviors and energy sequences are calculated and displayed in Figs. 9 and 10.

From Figs. 9 and 10, we can observe that different dynamical behaviors correspond to different energy distributions. Moreover, in both the chaotic state and

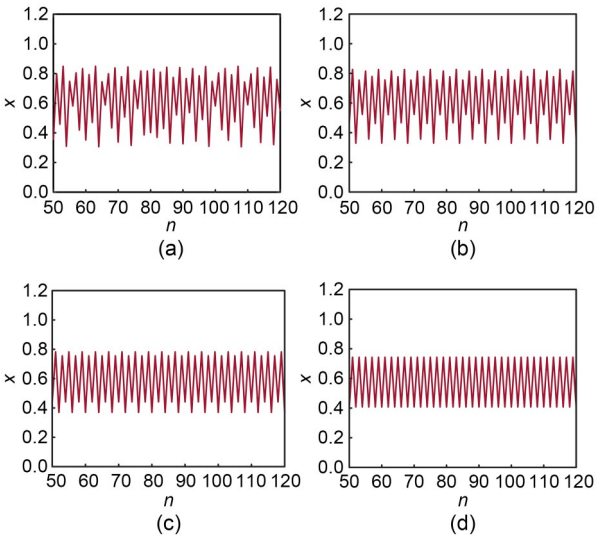

Fig. 9 Evolution of x under different values of parameter b: (a) b=0.55, a=1.5; (b) b=0.63, a=1.5; (c) b=0.73, a=1.5; (d) b=0.78, a=1.5

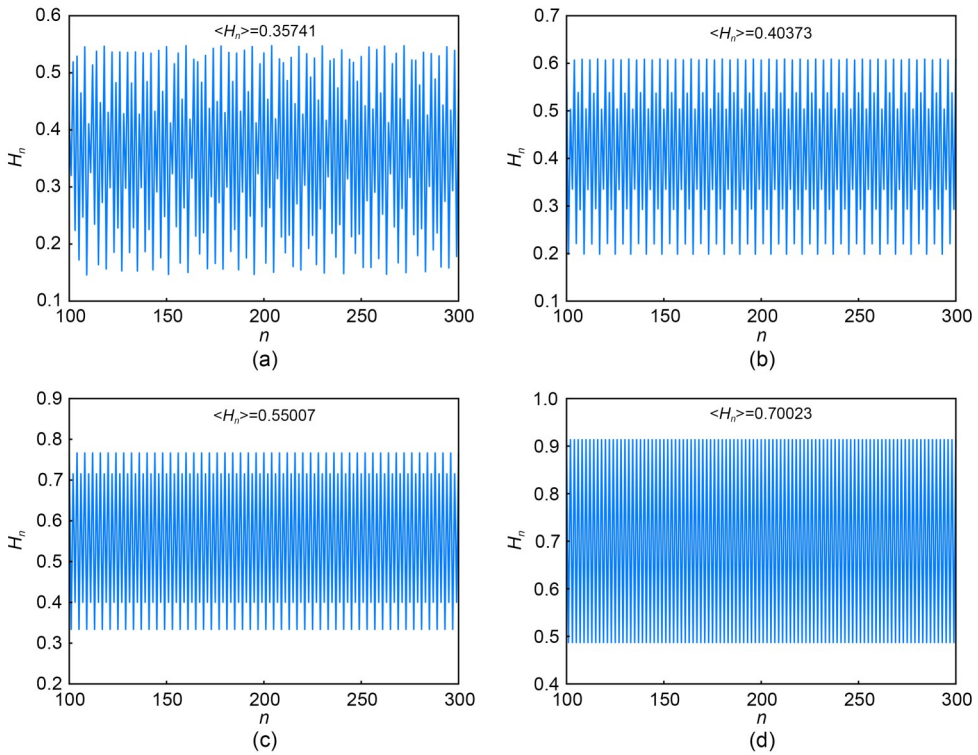

Fig. 10 Evolution of the Hamilton energy and its average value in the memristive map under different values of parameter b: (a) b=0.55, a=1.5; (b) b=0.63, a=1.5; (c) b=0.73, a=1.5; (d) b=0.78, a=1.5. <H_n> is the average value of the Hamilton energy

periodic state, there is a relatively small average energy value. Notably, as the number of cycles decreases, the average energy value keeps increasing. Next, to explore the energy regulation of the dynamics of the map system, an energy-controlled adaptive regulation criterion is defined as follows:

$$\begin{aligned} b &= b_0 + g \cdot \theta(\varepsilon - H_n), \\ \theta(v) &= 1, \ v \geq 0, \\ \theta(v) &= 0, \ v < 0, \end{aligned} \tag{31}$$

where b_0 is the initial value of the parameter b, g denotes a gain, ε is a threshold value, and parameter growth is controlled by applying the Heaviside function θ. The parameters are fixed at $\mu_1=\mu_2=3.9$, $c=0.12$, $a=1.5$, $\varepsilon=1.5$, and the initial value is (0.1, 0.2). The phase diagram, the growth of parameter b, and the y-variable sequence and energy sequence are shown in Fig. 11.

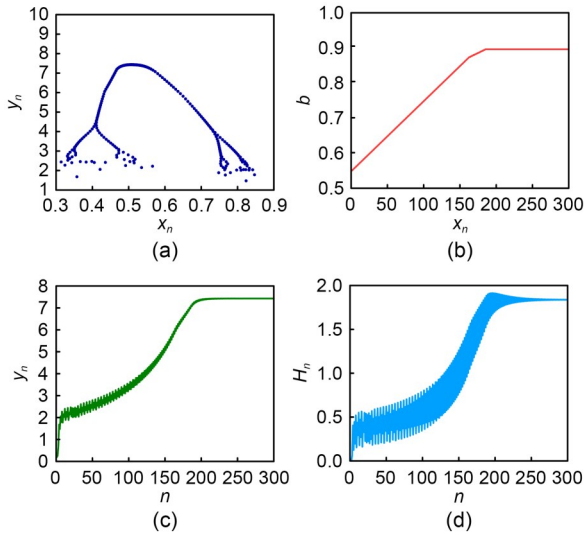

Fig. 11 (a) Phase portraits; (b) growth of parameter b; (c) evolution of variable y_n; (d) evolution of energy. The parameters are selected as g=0.002, b_0=0.55, ε=1.5, and an initial value of (0.1, 0.2)

The results show that parameter a reaches a stable value of 0.888 after 190 iterations under the gain g= 0.002. Moreover, chaotic states are suppressed to present periodic states, and the chaotic attractor evolves into periodic attractors.

In summary, a discrete chaotic system represented by a mathematical model can be expressed physically using a nonlinear memristor-based circuit composed of various electronic components. The energy function associated with the chaotic map system can be derived from its corresponding memristor-coupled circuit configurations. The main steps for circuit-based verification of a discrete chaotic system are as follows:

Step 1: A map model is derived in the form of a continuous differential equation through a linear transformation of the variables.

Step 2: Dimensionless continuous differential equations are defined in specific dimensions by applying the dimensions of the physical components (capacitor, inductor, memristor, and resistor).

Step 3: The differential equation is simplified following the dimension definition.

Step 4: The possible current or voltage relationships between the electronic components are obtained by applying Kirchhoff's law and the simplified dimensional differential equation.

Step 5: Design series-parallel circuits that can express the dimensional equations and satisfy Kirchhoff's law.

However, it should be noted that the present study has a few limitations. Firstly, potential synchronization between analog and digital chaotic systems was not investigated. Secondly, there were no simulations (such as in PSPICE, MATLAB, or Simulink), transient waveforms, or operating data used to validate the memristor-coupled circuits. Simulated oscilloscope-style outputs could be generated in future studies to perform further validation. Finally, we have not yet made detailed tests and comparisons of design complexity, parameter tunability, availability of energy functions, and hardware feasibility with recent chaos-to-circuit frameworks. In subsequent work these limitations will be addressed.

5 Conclusions

In this study, a 2D chaotic map was built using an open-loop modulation coupling method. The dynamical behaviors of the chaotic map showcased how both chaotic and diverse periodic patterns can be induced by adjusting the parameter values. Moreover, it was revealed that the 2D chaotic map can be implemented experimentally using two distinct memristor-coupled circuits. Our results indicate that higher-order terms in any 2D chaotic system can be equivalently realized

using a nonlinear resistor, while nonlinear cross terms and linear coupling between variables can be effectively represented by a memristor. Furthermore, the dimensional consistency of dimensionless equations can be restored through appropriate combinations of capacitance and resistance, or inductance and resistance. And notably, the energy function associated with a chaotic map system can be derived from its corresponding memristor-coupled circuit configurations. The circuit expression framework proposed in this study offers a generalized approach useful for hardware implementation and validation of other chaotic map systems.

Acknowledgments

This work is supported by the National Natural Science Foundation of China (No. 62301416). We are grateful to Prof. Jun MA (Lanzhou University of Technology, China) for his guidance on this work.

Author contributions

Feifei YANG edited the main text, methodology, and final version. Xinlin SONG provided supervision, software, and data analysis. Jia HE completed the data analysis. Huiping YIN was responsible for funding acquisition and supervision.

Conflict of interest

Feifei YANG, Xinlin SONG, Jia HE, and Huiping YIN declare that they have no conflict of interest.

References

Akraam M, Rashid T, Zafar S, 2023. A chaos-based image encryption scheme is proposed using multiple chaotic maps. *Mathematical Problems in Engineering*, 2023(1): 2003724. https://doi.org/10.1155/2023/2003724

Alexan W, Chen YL, Por LY, et al., 2023a. Hyperchaotic maps and the single neuron model: a novel framework for chaos-based image encryption. *Symmetry*, 15(5):1081. https://doi.org/10.3390/sym15051081

Alexan W, Alexan N, Gabr M, 2023b. Multiple-layer image encryption utilizing fractional-order chen hyperchaotic map and cryptographically secure prngs. *Fractal and Fractional*, 7(4):287. https://doi.org/10.3390/fractalfract7040287

Bao H, Hua ZY, Li HZ, et al., 2021. Discrete memristor hyperchaotic maps. *IEEE Transactions on Circuits and Systems I: Regular Papers*, 68(11):4534-4544. https://doi.org/10.1109/Tcsi.2021.3082895

Chen YX, Yang FF, Wang CN, 2025. Coherence resonance in a memristive map neuron and adaptive energy regulation. *Modern Physics Letters B*, 39(17):2550008. https://doi.org/10.1142/S0217984925500083

Gabr M, Korayem Y, Chen YL, et al., 2023. R^3—rescale, rotate, and randomize: a novel image cryptosystem utilizing chaotic and hyper-chaotic systems. *IEEE Access*, 11: 119284-119312. https://doi.org/10.1109/Access.2023.3326848

Gabr M, Diab A, Elshoush HT, et al., 2024. Data security utilizing a memristive coupled neural network in 3D models. *IEEE Access*, 12:116457-116477. https://doi.org/10.1109/Access.2024.3447075

Gao S, Zhang ZY, Iu HHC, et al., 2025. A parallel color image encryption algorithm based on a 2-D Logistic-Rulkov neuron map. *IEEE Internet of Things Journal*, 12(11): 18115-18124. https://doi.org/10.1109/JIOT.2025.3540097

Guo YT, Xie Y, Ma J, 2023. How to define energy function for memristive oscillator and map. *Nonlinear Dynamics*, 111(23):21903-21915. https://doi.org/10.1007/s11071-023-09039-9

Guo YT, Ma J, Zhang XF, et al., 2024. Memristive oscillator to memristive map, energy characteristic. *Science China Technological Sciences*, 67(5):1567-1578. https://doi.org/10.1007/s11431-023-2637-1

Hua ZY, Zhou YC, Pun CM, et al., 2015. 2D sine logistic modulation map for image encryption. *Information Sciences*, 297:80-94. https://doi.org/10.1016/j.ins.2014.11.018

Ibarz B, Casado JM, Sanjuán MAF, 2011. Map-based models in neuronal dynamics. *Physics Reports*, 501(1-2):1-74. https://doi.org/10.1016/j.physrep.2010.12.003

Jackson J, Perumal R, 2025. A robust image encryption technique based on an improved fractional order chaotic map. *Nonlinear Dynamics*, 113(7):7277-7296. https://doi.org/10.1007/s11071-024-10480-7

Jia JN, Wang CN, Zhang XF, et al., 2024. Energy and self-adaption in a memristive map neuron. *Chaos, Solitons & Fractals*, 182:114738. https://doi.org/10.1016/j.chaos.2024.114738

Lai Q, Liu Y, 2023. A cross-channel color image encryption algorithm using two-dimensional hyperchaotic map. *Expert Systems with Applications*, 223:119923. https://doi.org/10.1016/j.eswa.2023.119923

Lei Z, Ma J, 2025. Coherence resonance and energy dynamics in a memristive map neuron. *Chaos*, 35(2):023158. https://doi.org/10.1063/5.0251352

Li KS, Wang Q, Hu CY, et al., 2024. Dynamical analysis of a novel 2D Lyapunov exponent controllable memristive chaotic map. *Chaos*, 34(8):083135. https://doi.org/10.1063/5.0187297

Li LZ, 2024. A novel chaotic map application in image encryption algorithm. *Expert Systems with Applications*, 252: 124316. https://doi.org/10.1016/j.eswa.2024.124316

Li YN, Lv M, Ma J, et al., 2024. A discrete memristive neuron and its adaptive dynamics. *Nonlinear Dynamics*, 112(9): 7541-7553. https://doi.org/10.1007/s11071-024-09361-w

Liu XC, Mou J, Zhang YS, et al., 2024. A new hyperchaotic map based on discrete memristor and meminductor: dynamics analysis, encryption application, and DSP implementation. *IEEE Transactions on Industrial Electronics*,

71(5):5094-5104.
https://doi.org/10.1109/Tie.2023.3281687

Luo LQ, Flanagan JG, 2007. Development of continuous and discrete neural maps. *Neuron*, 56(2):284-300.
https://doi.org/10.1016/j.neuron.2007.10.014

Ma ML, Yang Y, Qiu ZC, et al., 2022. A locally active discrete memristor model and its application in a hyperchaotic map. *Nonlinear Dynamics*, 107(3):2935-2949.
https://doi.org/10.1007/s11071-021-07132-5

Ma YJ, Tian Y, Zhang L, et al., 2024. Two-dimensional hyperchaotic effect coupled mapping lattice and its application in dynamic S-box generation. *Nonlinear Dynamics*, 112(19):17445-17476.
https://doi.org/10.1007/s11071-024-09907-y

Muni SS, Fatoyinbo HO, Ghosh I, 2022. Dynamical effects of electromagnetic flux on Chialvo neuron map: nodal and network behaviors. *International Journal of Bifurcation and Chaos*, 32(9):2230020.
https://doi.org/10.1142/S0218127422300208

Narayanan R, Johnston D, 2012. Functional maps within a single neuron. *Journal of Neurophysiology*, 108(9):2343-2351.
https://doi.org/10.1152/jn.00530.2012

Peng YX, Sun KH, He SB, 2020. Dynamics analysis of chaotic maps: from perspective on parameter estimation by metaheuristic algorithm. *Chinese Physics B*, 29(3):030502.
https://doi.org/10.1088/1674-1056/ab695c

Peng YX, He SB, Sun KH, 2021. A higher dimensional chaotic map with discrete memristor. *AEU-International Journal of Electronics and Communications*, 129:153539.
https://doi.org/10.1016/j.aeue.2020.153539

Peng YX, Lan ZX, Sun KH, et al., 2023. A simple color image encryption algorithm based on a discrete memristive hyperchaotic map and time-controllable operation. *Optics & Laser Technology*, 165:109543.
https://doi.org/10.1016/j.optlastec.2023.109543

Ramakrishnan B, Mehrabbeik M, Parastesh F, et al., 2022. A new memristive neuron map model and its network's dynamics under electrochemical coupling. *Electronics*, 11(1):153.
https://doi.org/10.3390/electronics11010153

Sameh SM, Moustafa HED, Abdelhay EH, et al., 2024. An effective chaotic maps image encryption based on metaheuristic optimizers. *The Journal of Supercomputing*, 80(1):141-201.
https://doi.org/10.1007/s11227-023-05413-x

Tutueva AV, Nepomuceno EG, Karimov AI, et al., 2020. Adaptive chaotic maps and their application to pseudorandom numbers generation. *Chaos, Solitons & Fractals*, 133:109615.
https://doi.org/10.1016/j.chaos.2020.109615

Umar T, Nadeem M, Anwer F, 2024. A new modified Skew Tent Map and its application in pseudo-random number generator. *Computer Standards & Interfaces*, 89:103826.
https://doi.org/10.1016/j.csi.2023.103826

Verma V, Kumar S, 2025. Quantum image encryption algorithm based on 3D-BNM chaotic map. *Nonlinear Dynamics*, 113(4):3829-3855.
https://doi.org/10.1007/s11071-024-10403-6

Wang BC, Zhang XF, Zhu ZG, et al., 2024. A new memristive map neuron, self-regulation and coherence resonance. *The European Physical Journal B*, 97(8):124.
https://doi.org/10.1140/epjb/s10051-024-00760-x

Wang C, Chong ZL, Zhang HL, et al., 2024. Color image encryption based on discrete memristor logistic map and DNA encoding. *Integration*, 96:102138.
https://doi.org/10.1016/j.vlsi.2024.102138

Wang P, Wang Q, Sang HW, et al., 2025. Dynamic analysis of a novel 3D chaotic map with two internal frequencies. *Scientific Reports*, 15(1):5952.
https://doi.org/10.1038/s41598-025-90596-x

Wang Z, Parastesh F, Natiq H, et al., 2024. Synchronization patterns in a network of diffusively delay-coupled memristive Chialvo neuron map. *Physics Letters A*, 514-515: 129607.
https://doi.org/10.1016/j.physleta.2024.129607

Wu WQ, Zhou JP, 2024. Constructing new high-order polynomial chaotic maps and application in pseudorandom number generator. *Physica Scripta*, 99(3):035238.
https://doi.org/10.1088/1402-4896/ad25d5

Xiang Q, Shen YZ, Peng SS, et al., 2024. A two-dimensional discrete memristor map: analysis and implementation. *International Journal of Bifurcation and Chaos*, 34(10): 2450124.
https://doi.org/10.1142/S0218127424501244

Xu Q, Huang LP, Wang N, et al., 2023. Initial-offset-boosted coexisting hyperchaos in a 2D memristive Chialvo neuron map and its application in image encryption. *Nonlinear Dynamics*, 111(21):20447-20463.
https://doi.org/10.1007/s11071-023-08905-w

Yang FF, Zhou P, Ma J, 2024a. An adaptive energy regulation in a memristive map linearized from a circuit with two memristive channels. *Communications in Theoretical Physics*, 76(3):035004.
https://doi.org/10.1088/1572-9494/ad260e

Yang FF, Song XL, Ma J, 2024b. A memristive map neuron under noisy electric field. *Chinese Journal of Physics*, 91: 287-298.
https://doi.org/10.1016/j.cjph.2024.07.035

Yang FF, Ren LJ, Ma J, et al., 2024c. Two simple memristive maps with adaptive energy regulation and digital signal process verification. *Journal of Zhejiang University-SCIENCE A*, 25(5):382-394.
https://doi.org/10.1631/jzus.A2300651

Zhang SH, Zhang HL, Wang C, 2023. Dynamical analysis and applications of a novel 2-D hybrid dual-memristor hyperchaotic map with complexity enhancement. *Nonlinear Dynamics*, 111(16):15487-15513.
https://doi.org/10.1007/s11071-023-08652-y